Electronic Supplementary Information

Effective dual-mode turn-on sensing of phosphates enabled by the twisted "head-to-head" self-assembly of Platinum(II)-terpyridyl complex with close Pt-Pt packing

Jiajia Xie,[a†] Fangfang Xiao,[b,c†] Chaogan Liu,[d] Jian Sun,[a] Jun Yao,[a*] Yushu Li[a*]

[a] College of Pharmacy, Xinjiang Key Laboratory of Biopharmaceuticals and Medical Devices, Xinjiang Medical University, Urumqi 830017, China.

[b] Xinjiang Key Laboratory of Trace Chemicals Sensing, Xinjiang Technical Institute of Physics & Chemistry, Chinese Academy of Sciences, Urumqi 830011, China.

[c] Center of Materials Science and Optoelectronics Engineering, University of Chinese Academy of Sciences, Beijing 100049, China.

[d] State Key Laboratory of Fine Chemicals, Frontiers Science Center for Smart Materials Oriented Chemical Engineering, Dalian University of Technology, Dalian 116024, China.

* Corresponding authors: xydyaojun2022@xjmu.edu.cn (J. Yao), liys@xjmu.edu.cn (Y. S. Li)

[†] These authors contributed equally to this work.

Experimental Section

Reagents and Materials

Unless otherwise noted, all reagents and materials were obtained from commercial sources and used without further purification. Ethyl ether ($C_4H_{10}O$) was obtained from Zhi Yuan (Tianjin, China). Ethanol (CH_3CH_2OH), ethyl acetate ($C_4H_8O_2$), dimethyl sulfoxide (DMSO), acetic acid (CH_3COOH), methanol (CH_3OH) were obtained from Xinbrete (Tianjin, China). Potassium tetrachloroplatinate(II) (K_2PtCl_4), 1,5-cyclooctadiene, sodium phosphate (Na_3PO_4), sodium metaphosphate ($Na_6O_{18}P_6$), ammonium chloride (NH_4Cl), calcium chloride ($CaCl_2$), manganese chloride ($MnCl_2$), sodium perchlorate ($NaClO_4$), ammonium hexafluorophosphate (NH_4PF_6), ammonium tetrafluoroborate (NH_4BF_4), sodium hexafluoroantimonate ($NaSbF_6$), and sodium nitrate ($NaNO_3$) were purchased from Aladdin Chemical Reagent Ltd. Sodium dihydrogen phosphate (NaH_2PO_4), sodium bicarbonate ($NaHCO_3$), sodium salicylate ($C_7H_5O_3Na$), magnesium chloride ($MgCl_2$), nickel chloride ($NiCl_2$), and hydrogen peroxide (H_2O_2) were purchased from Hongyan (Tianjin, China). Disodium hydrogenorthophosphate (Na_2HPO_4) was purchased from OuBoKai (Tianjin, China). Sodium pyrophosphate ($Na_4O_7P_2$) was purchased from Bide (Shanghai, China). Adenosine-5′-diphosphate (ADP), adenosine triphosphate (ATP), 4′-Hydroxy-2,2′:6′,2′′-Terpyridine were purchased from Macklin (Shanghai, China). Sodium acetate (AcONa), and calcium chloride ($CaCl_2$) were obtained from Baishi (Tianjin, China). Sodium nitrite ($NaNO_2$) was obtained from Kemeng (Tianjin, China). Potassium chloride (KCl) was obtained from Guangfu (Tianjin, China). Cobaltous chloride ($CoCl_2$) was obtained from Fuchen (Tianjin, China). Sodium hypochlorite (NaClO) was obtained from Alfa Aesar. The solutions were prepared using ultrapure deionized water (18.2 MΩ).

Characterization

^{1}H NMR spectra were obtained on Bruker Avance NEO 400MHz with DMSO-d_6 as a deuterated solvent. Mass spectra were determined with a Q Exactive-type four-stage rod-Orbitrap high-resolution mass spectrometer (HRMS, UHPLC-Q-Orbitrap-HRMS, Thermo Fisher Scientific). The single crystal X-ray diffraction data were collected on a Bruker d8 venture metaljet photon II diffractometer and Olex2 software was used to solve the structure. Ultraviolet-visible absorption spectra were measured on Hitachi UV-3900 ultraviolet-visible spectrophotometer using 1 cm quartz cuvettes. Emission spectra were obtained on an Edinburgh FLS1000 photoluminescence spectrometer. The temperature-dependent photophysical properties of thin films were acquired in an Oxford optistatDN cryostat situated in the cell compartment of the Edinburgh FLS980 spectrophotometer. Field-emission scanning electron microscopy (JEOL JSM-7610F Plus, 5 kV) and transmission electron microscope (JEM-P200, HRP, 200 kV) were used to characterize the morphology and the detailed structure of the samples. Dynamic light scattering analyses were measured on Malvern Zetasizer Nano ZS90. The digital photographs were recorded on an iPhone 13 or an industrial camera (Mars 5000s-20gc, Vision Datum).

The optical micrographs were recorded on a Nikon Eclipse Ti2 microscope equipped with an IMG SD1600A camera.

Synthesis process of [Pt(tpy-OH)Cl]·Cl, [Pt(tpy-CHO)Cl]·Cl, and [Pt(tpy-H)Cl]·Cl

[Pt(tpy-OH)Cl]·Cl , [Pt(tpy-CHO)Cl]·Cl, and [Pt(tpy-H)Cl]·Cl were synthesized through a modified route according to previous methods[1],[2] as shown in Scheme S1.

Synthesis of $Pt(COD)Cl_2$

To a round bottom flask charged with 20 ml DI water, potassium chloroplatinate (0.5 g, 2.409 mmol) was added first, and after 10 minutes acetic acid (24 ml) and 1,5-cyclooctadiene (2.4 ml, 18.66 mmol) were added in sequence under stirring at room temperature. The mixed solution was then refluxed at 85 °C for 3 h under stirring. After cooling down to room temperature, the mixture was filtered and rinsed with water, ethanol, and ether three times respectively. The residue was then dried in an oven at 45 °C to yield $Pt(COD)Cl_2$ as a bright gray solid for direct use in the next step.

Synthesis of [Pt(tpy-OH)Cl]·Cl

The 50 ml round bottom flask was charged with $Pt(COD)Cl_2$ (0.3018 g, 0.8066 mmol), 4'-Hydroxy-2,2':6',2''-Terpyridine (0.2012 g, 0.7585 mmol), and 20 ml DI water. The mixed solution was then stirred continuously at 45 °C for 24 h until pale yellowish-green precipitates formed. After cooling to room temperature, the residue was filtered and washed with ethyl ether followed by drying in the oven at 45 °C. ^{1}H NMR (400 MHz, DMSO-d_6) δ 8.90 (d, *J* = 5.8 Hz, 2H), 8.41 (d, *J* = 4.5 Hz, 4H), 7.84 (q, *J* = 5.0 Hz, 2H), 7.54 (s, 2H). HRMS: Calcd. for 480.02; Found 480.02.

Synthesis of [Pt(tpy-CHO)Cl]·Cl

The 50 ml round bottom flask was charged with $Pt(COD)Cl_2$ (0.1500 g, 0.4000 mmol), 4'-Formyl-2,2':6',2''-terpyridine (0.1040 g, 3.980 mmol), and 10 ml DI water. The mixed solution was then stirred continuously at 45 °C for 15 min. After cooling to room temperature, the mixture was filtered and the filtrate was then concentrated via rotavapor. The solid obtained was then washed with ethyl ether and cold ethanol for three times to yield the final product. ^{1}H NMR (600 MHz, D_2O) δ 8.09 (td, J = 7.7, 1.5 Hz, 2H), 8.02 (s, 2H), 7.96 (d, J = 5.4 Hz, 2H), 7.92 (d, J = 7.9 Hz, 2H), 7.46 – 7.37 (m, 2H), 6.00 (s, 1H). HRMS: Calcd. for 492.02; Found 492.02.

Synthesis of [Pt(tpy-H)Cl]·Cl

The 50 ml round bottom flask was charged with $Pt(COD)Cl_2$ (0.1500 g, 0.4000 mmol), 2,2':6',2''-terpyridine (0.0094 g, 3.980 mmol), and 10 ml DI water. The mixed solution was then stirred continuously at 45 ℃ for 15 min. After cooling to room temperature, the mixture was filtered, the filtrate was collected, and then concentrated via rotavapor. The solid obtained was then washed with ethyl ether three times to yield the final product. ^{1}H NMR (400 MHz, DMSO-d_6) δ 8.85 (d, *J* = 5.7 Hz,2H), 8.61 (m, J = 6.6 Hz, 5H), 8.50 (t, *J* = 7.9 Hz, 2H), 7.94 (t, J = 6.6 Hz, 2H). HRMS: Calcd. for 465.03; Found 465.03.

Preparing single crystals and X-ray crystallography

Preparation of [Pt(tpy-OH)Cl]·Cl probe single crystal

Ethyl acetate was slowly diffused into a saturated DMSO solution of [Pt(tpy-OH)Cl]·Cl at room temperature to obtain crystals. Yellow [Pt(tpy-OH)Cl]·Cl crystals are mounted randomly on the glass fiber. The single crystal X-ray diffraction (SXRD) data were collected by W-scanning at 204 K on a Bruker D8 VENTURE Metaljet PHOTON II diffractometer. The crystal was kept at 204.00 K during data collection. Using Olex2[3], the structure was solved with the SHELXT[4] structure solution program using Intrinsic Phasing and refined with the SHELXL[5] refinement package using Least Squares minimization.

Preparation of the product single crystal

The X-ray quality single crystal of [Pt(tpy-OH)Cl] was obtained by slow evaporation of its saturated methanol solution at room temperature. Yellow [Pt(tpy-OH)Cl] crystals are mounted randomly on the glass fiber. Single crystal X-ray diffraction (SXRD) data were collected by W-scanning at 193.00 K on a Bruker D8 VENTURE Metaljet diffractometer. The crystal was kept at 193.00 K during data collection. Using Olex2[6], the structure was solved with the olex2. Solve[7] structure solution program using Charge Flipping and refined with the olex2. Refine[7] refinement package using Gauss-Newton minimization.

Preparation of sample and testing process

Preparation of [Pt(tpy-OH)Cl]·Cl probe solution (0.6 mM)

The 0.6 mM [Pt(tpy-OH)Cl]·Cl probe solution was obtained by dissolving 0.0247 g [Pt(tpy-OH)Cl]·Cl in 80 ml mixed solution consisting of acetic acid:ethanol:water=1:2:5 with ultrasonic assistance.

Preparation of [Pt(tpy-OH)Cl]·Cl probe solution (0.6 mM) with various PH value

The 0.6 mM [Pt(tpy-OH)Cl]·Cl probe solution was obtained by dissolving 0.0247 g [Pt(tpy-OH)Cl]·Cl in 80 ml mixed solution consisting of acetic acid:ethanol:water=1:2:5 with ultrasonic assistance as pH=3, and using 1M HCl and NaOH to adjust the pH to 2, 2.5, 3.5, 4.

Preparation of phosphate solution with various concentrations

The sodium phosphate (1.63 g) was dissolved in deionized water (10 ml) to prepare a sodium phosphate solution with a concentration of 1 M. Then the solution was diluted with deionized water to obtain various concentrations of sodium phosphate solutions in the range of 0-0.01 M.

Spectral response testing

200 μL of sodium phosphate solution (0.3, 0.5, 0.8, 1, 1.2, 1.5, 1.8, 2, 3, 4, 5, 6, 7, 8, 9, 10 mM, respectively) was added into 1.8 ml of the [Pt(tpy-OH)Cl]·Cl probe solution. The fluorescence detection performance of phosphate was recorded with Edinburgh FLS1000 fluorescence spectrophotometer.

Ultraviolet-visible absorption spectra were measured on Hitachi UV-3900 ultraviolet-visible spectrophotometer.

Preparation and testing of other analytes by [Pt(tpy-OH)Cl]·Cl probe

Preparation of analyte solutions (0.1 and 0.2 M): Na_3PO_4, NaH_2PO_4, Na_2HPO_4, $(NaPO_3)n$, $Na_4O_7P_2$, ADP, ATP, $NaBrO_3$, AcONa, Na_2CO_3, $NaHCO_3$, $NaNO_3$, $NaNO_2$, $C_7H_5O_3Na$, KCl, NH_4Cl, $CaCl_2$, $MgCl_2$, $CoCl_2$, $MnCl_2$, $NiCl_2$, NaClO, H_2O_2, $NaClO_4$, NH_4PF_6, NH_4BF_4 and $NaSbF_6$ were dissolved in deionized water to prepare the analyte solution with a concentration of 0.1 and 0.2 M.

^{1}H NMR tritration experiment: Prepare the 0.6 mM[Pt(tpy-OH)Cl]Cl probe solution using detuerated solution ($C_2H_3DO_2$:C_2H_5DO:D_2O=1:2:5, V/V) and the Na_3PO_4 (5 mM) in D_2O, respectively. Charge the NMR tube with the [Pt(tpy-OH)Cl]Cl (500 μL, 0.6 mM) and continously add Na_3PO_4 (5 mM) with volume step of 20 μL for 5 times, record the ^{1}H NMR spectra.

Selectivity testing process: The solution (0.1 M, 200 μL) of a certain analyte was added into a centrifuge tube filled with 1.8 ml of the [Pt(tpy-OH)Cl]·Cl probe solution (0.6 mM). After the reaction, the fluorescence spectra and images were measured and recorded.(λ_{ex} = 365 nm; slit width: 2 nm; λ_{em} = 715 nm; slit width:3 nm; Spectrometer: Edinburgh FLS1000). Absorption spectra and images were measured and recorded (Scan speed: 600 nm/min; Sampling interval: 0.5 nm; Replicates: 1; Slit width: 1nm).

Anti-interference testing process: The mixture of the certain analyte (0.2 M, 100μL) and phosphate (0.2 M, 100μL) was added into a centrifuge tube filled with 1.8 ml of the [Pt(tpy-OH)Cl]·Cl probe solution (0.6 mM). After the reaction, the fluorescence spectra and images were measured and recorded.(λ_{ex} = 365 nm; slit width: 2 nm; λ_{em} = 715 nm; slit width:3 nm; Spectrometer: Edinburgh FLS1000). Absorption spectra and images were measured and recorded (Scan speed: 600 nm/min; Sampling interval: 0.5 nm; Replicates: 1; Slit width: 1nm).

Fluorescence microscopy of the product: 200 μL sodium phosphate solution (0.3 mM) was added to 1.8 ml [Pt(tpy-OH)Cl]·Cl probe solution (0.6 mM), and the colorimetric and fluorescent micrographs were recorded after the mixture was kept for half an hour.

Preparation of product sample for morphology characterization:

SEM and TEM samples: 2 ml of phosphate solution (3 mM) was added to 18 ml diluted [Pt(tpy-OH)Cl]·Cl probe solution (0.3 mM), followed by steadily standing for two hours. The mixture was centrifuged and washed with acetic acid/ethanol/water (1:2:5, v/v) solution for 5 times, and the final supernatant was drop cast onto the silica or copper substrate for SEM and TEM characterization.

Preparation of the [Pt(tpy-OH)Cl]·Cl porous polymer sensing chip

Ten tablets of PE absorbent materials (3×3×3 mm) were soaked in 20 ml of mixture (acetic acid:ethanol:water=1:2:5) overnight first. The pretreated PE absorbent materials were then soaked in

0.5 mM [Pt(tpy-OH)Cl]·Cl probe solution (20 ml) for 3 hours, and finally soaked in another 0.5 mM [Pt(tpy-OH)Cl]·Cl probe solution (20 ml) for 24 hours.

Phosphate solution:

The sodium phosphate (1.63 g) was dissolved in deionized water (10 ml) to prepare a sodium phosphate solution with a concentration of 1 M. Then the solution was diluted with deionized water to obtain various concentrations of sodium phosphate solutions

Analyte solutions (0.001 M): Na_3PO_4, NaH_2PO_4, Na_2HPO_4, $(NaPO_3)n$, $Na_4O_7P_2$, ADP, ATP, $NaBrO_3$, AcONa, Na_2CO_3, $NaHCO_3$, $NaNO_3$, $NaNO_2$, $C_7H_5O_3Na$, KCl, NH_4Cl, $CaCl_2$, $MgCl_2$, $CoCl_2$, $MnCl_2$, $NiCl_2$, NaClO, H_2O_2, $NaClO_4$, NH_4PF_6, NH_4BF_4 and $NaSbF_6$ were dissolved in deionized water to prepare the analyte solution with a concentration of 0.001 M.

Sensing testing of the sensor unit for Phosphate solution: Different concentrations of phosphate solutions were firstly prepared to be 0, 100, 300, 400, 500, 600, 800, 900,1000 μM, respectively. Then, the above phosphate solution of μL was measured with a pipette gun and added to a sensor unit, After 90 s, Fluorescent and colorimetric images were measured and recorded with a digital camera

Selectivity testing process: The solution (0.001 M, 7 μL) of a certain analyte was added to the [Pt(tpy-OH)Cl]·Cl] porous polymer sensor chip. After 90 s, Fluorescent and colorimetric images were measured and recorded with a digital camera.

Computational details

Construction of Initial Structure: The initial molecular structure selected in this study is derived from the crystal database, with the molecular structure unit chosen for subsequent computations and analyses. The model was constructed using GaussView 6.0 software.

Experimental Principles: The reaction barrier (ΔE) represents the molar energy difference between the activated complex and the ground-state energy level of reactant molecules. The height of the reaction barrier determines the difficulty level of the chemical reaction.

$\Delta E_{TS} = E_{TS} - E_{Reactant}$

Where ΔE_{TS} denotes the energy of the transition state, and $E_{Reactant}$ represents the ground-state energy of the reactant. Both quantities are expressed in kJ/mol.

Computational Methods:

The reactants and products studied in this research employed the B3LYP method of Density Functional Theory (DFT)[8], utilizing the all-electron basis set DEF2SVP.[9],[10] Molecular structures were further optimized to convergence, zero-point energy correction was applied, and the Solvation Model Density (SMD) was employed with water as the solvent. This method allows for accurate modeling of solvent effects within the framework of density functional theory.[11] The transition states were obtained using the TS method at the same method and basis set level, and potential transition states were confirmed through vibrational analysis. ESP were finished by Multiwfn 3.4.1,[12] which is a

multifunctional wavefunction analysis program. All isosurface maps were rendered by VMD 1.9.1 program[13] based on the outputs of Multiwfn. During the quantitative analyses of the electrostatic potential on van der Waals (vdW) surface in Multiwfn program, the grid spacings were set to 0.2 bohr, which are slightly fner than the default settings and hence can lead to more accurate results. All the aforementioned computations were conducted using the Gaussian 16 software package.[14]

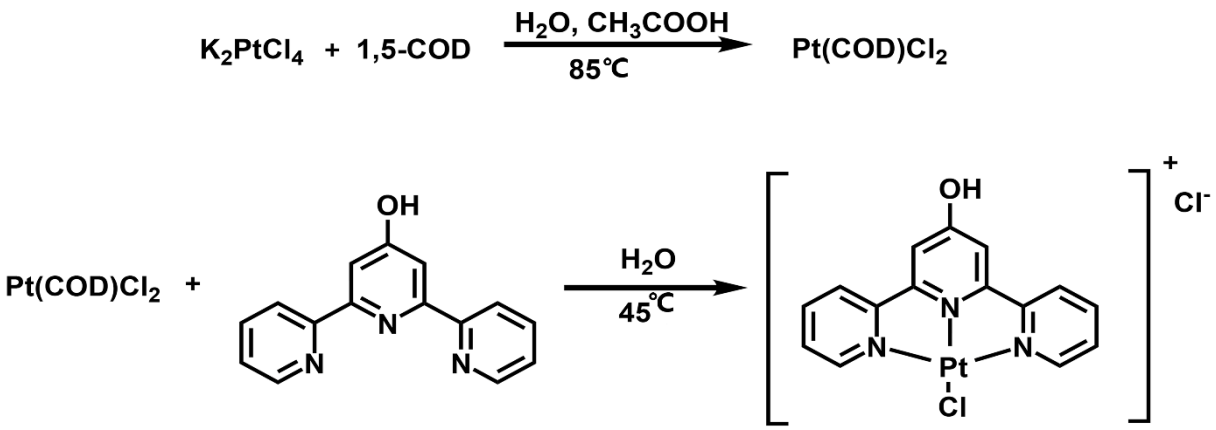

Scheme S1. Synthetic procedures of the probe

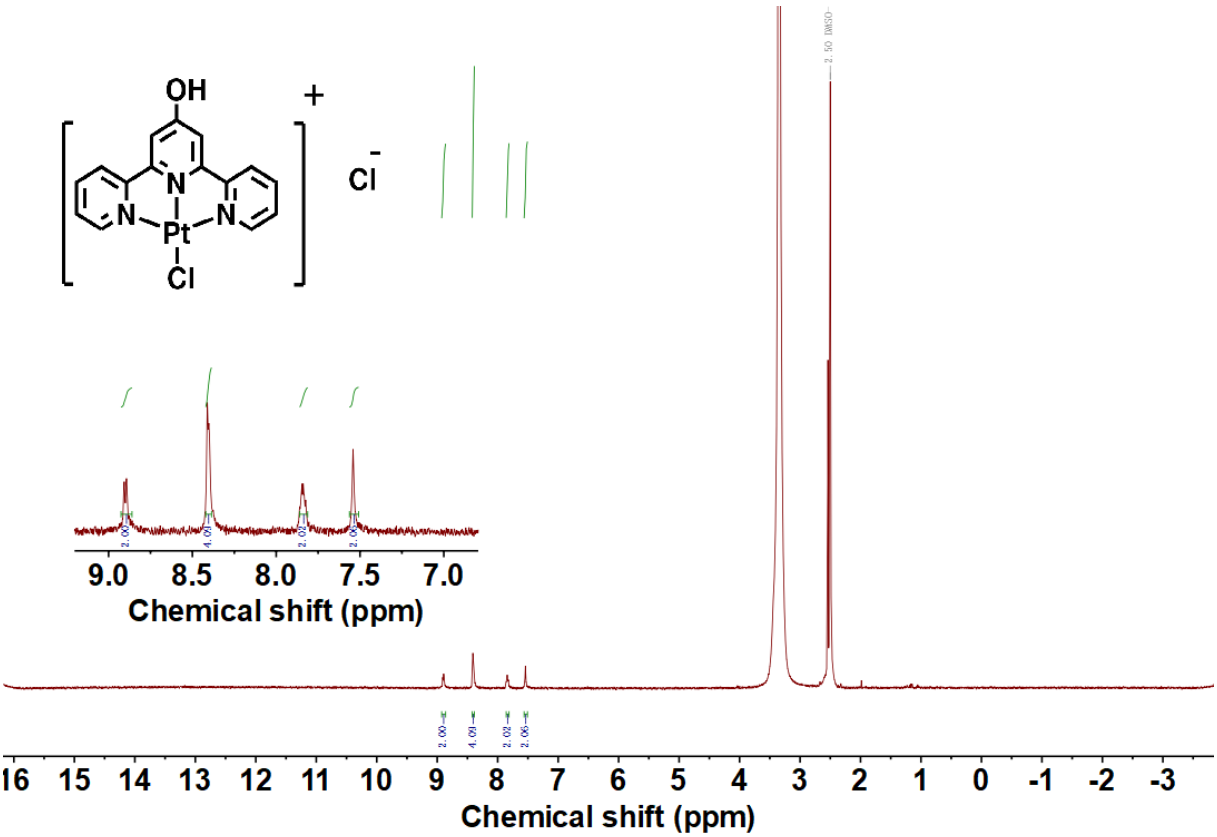

Figure S1. ^{1}H NMR spectra of the probe

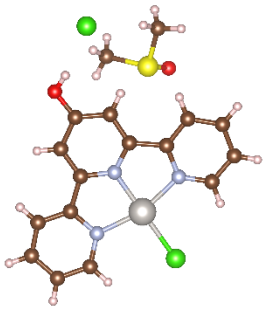

Figure S2. Single crystal structure of the probe

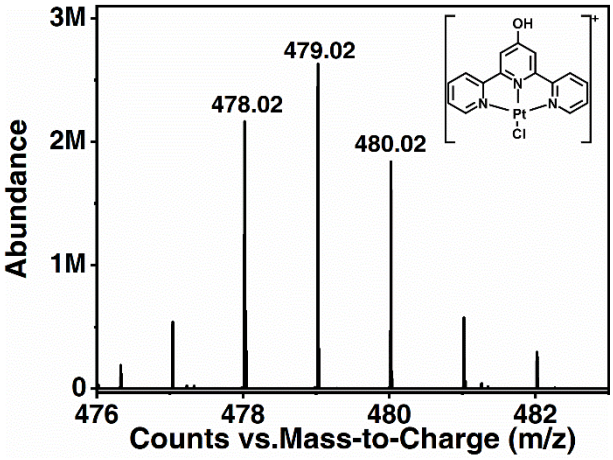

Figure S3. HRMS spectra of the probe

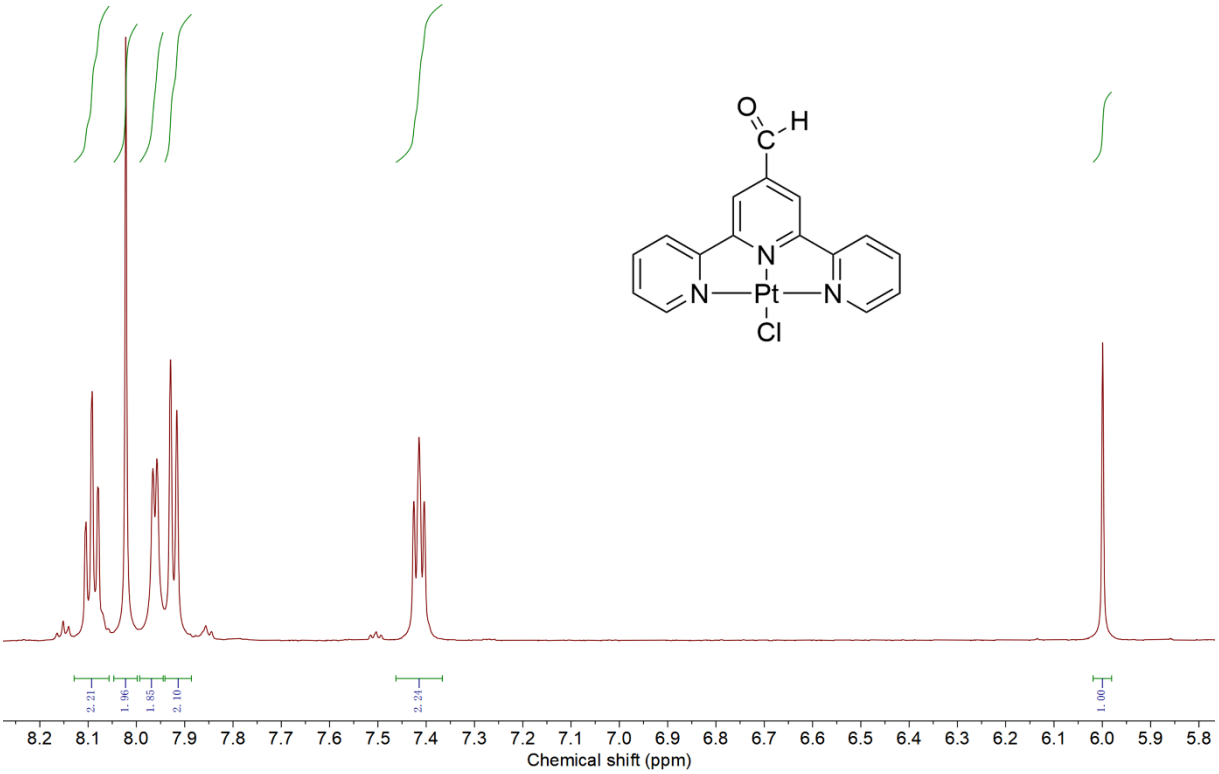

Figure S4. ^{1}H NMR spectra of the -CHO probe

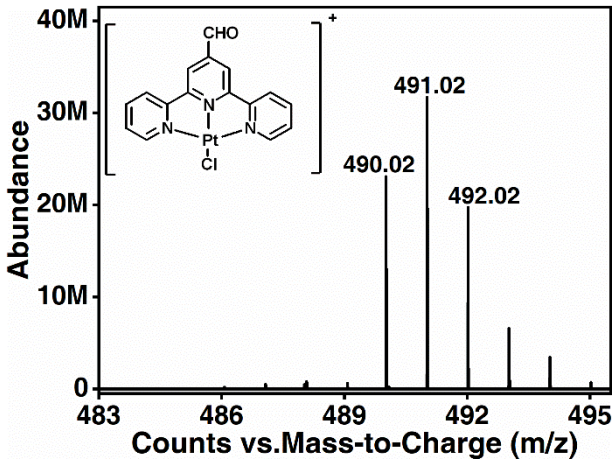

Figure S6. HRMS spectra of the -CHO probe

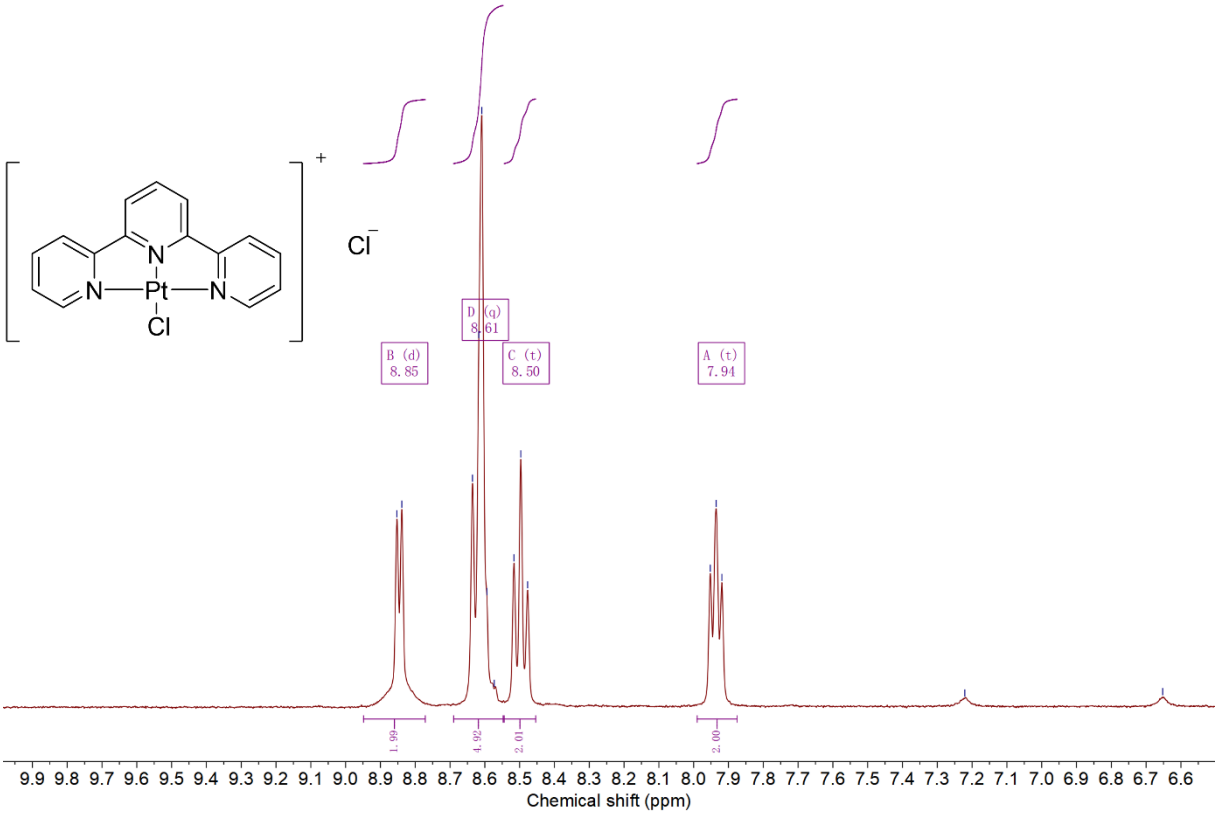

Figure S5. ^{1}H NMR spectra of the -H probe

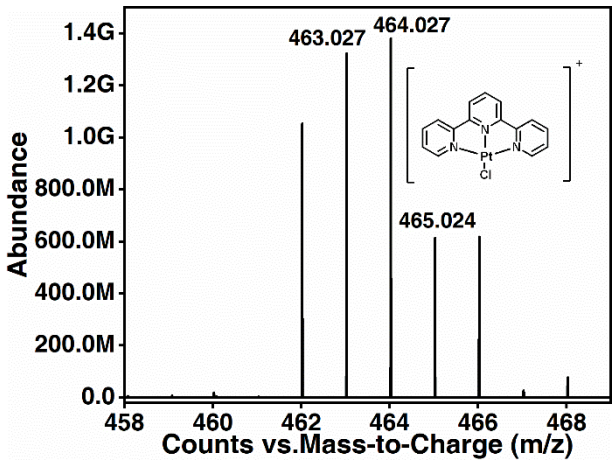

Figure S7. HRMS spectra of the -H probe

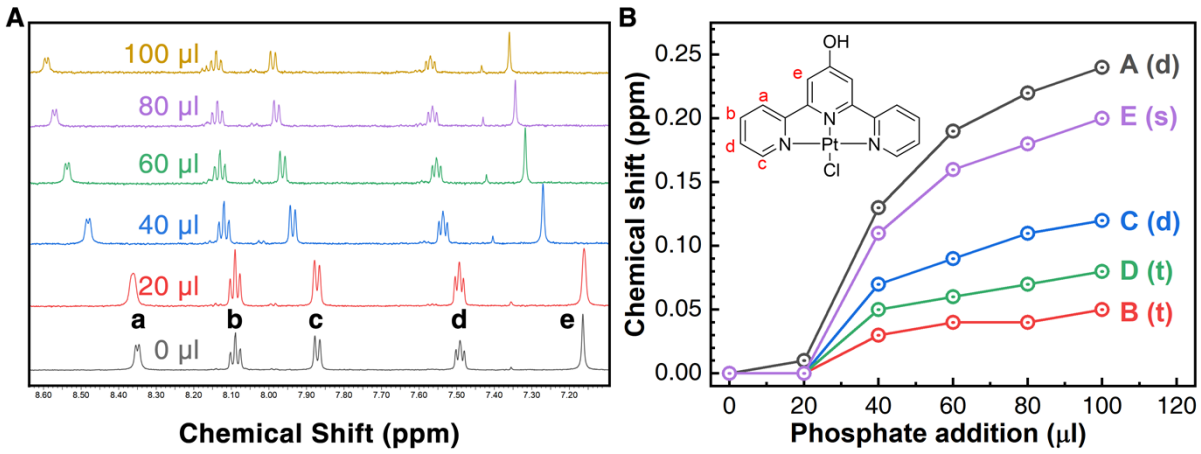

Figure S8. The NMR titration experiment with continuous increasing addition amount of phosphate solution (5 mM in D_2O) into the [Pt(tpy-OH)Cl]·Cl solution (0.6 mM in deuterated-solvent mixture) in-situ reacted in the NMR tube

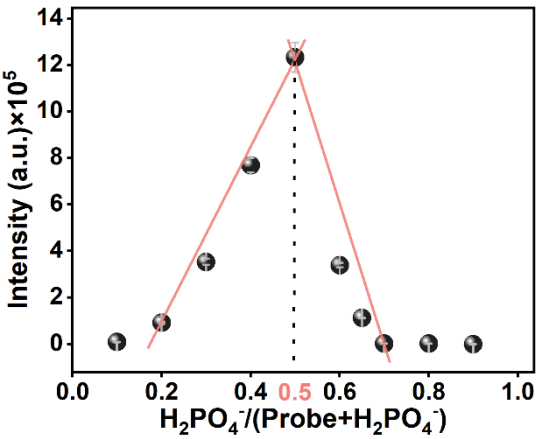

Figure S9. The Job's plot monitored at the emission wavelength of 715 nm for the tritration experiment by mixing [Pt(tpy-OH)Cl]Cl and Na_3PO_4 in the mixture solution (AcOH:EtOH:H2O=1:2:5, V/V)

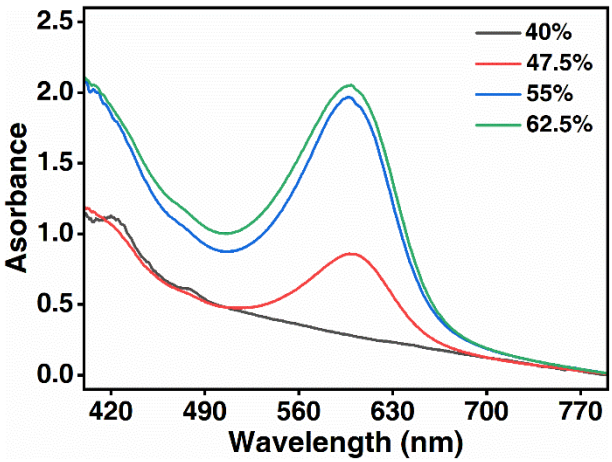

Figure S10. The absorption spectra of the[Pt(tpy-OH)Cl]·Cl solution with different water contants after adding same amount of sodium phosphate solution

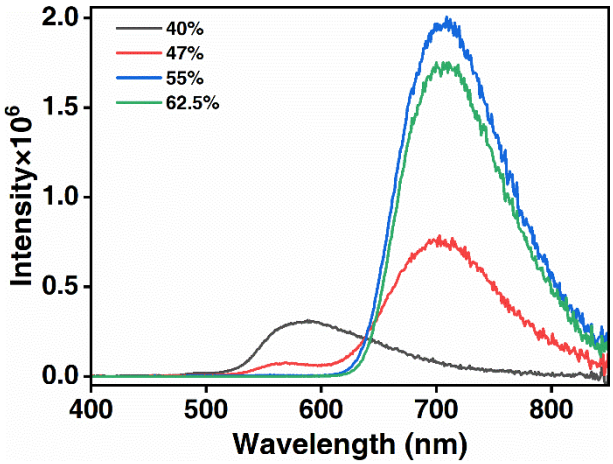

Figure S11. The emission spectra of the [Pt(tpy-OH)Cl]·Cl solution with different water contants after adding same amount of sodium phosphate solution

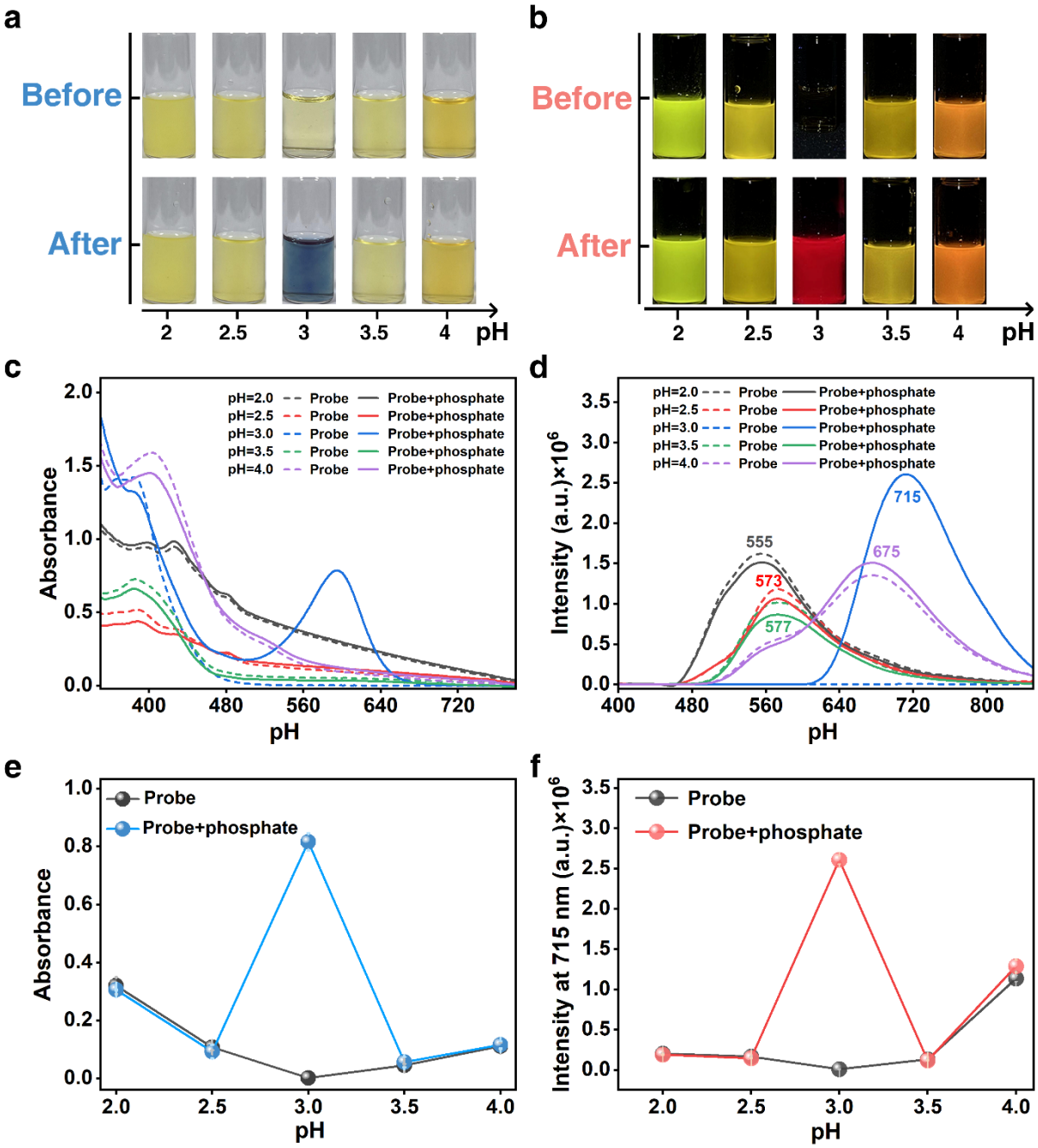

Figure S12. The effects of pH on the sensing performance towards phosphate: a) the sunlight images; b) the dark field images under 365 nm irradiation; c) the UV-vis absorption spectra; d) the fluorescent emission spectra with excitation at 365 nm; e) the corresponding absorbance change at 597 nm; and f) the corresponding FL intensity change at 715 nm of the probe solution (0.6 mM, 1.8 ml) with different pH before and after adding phosphate (1 mM, 200 μl)

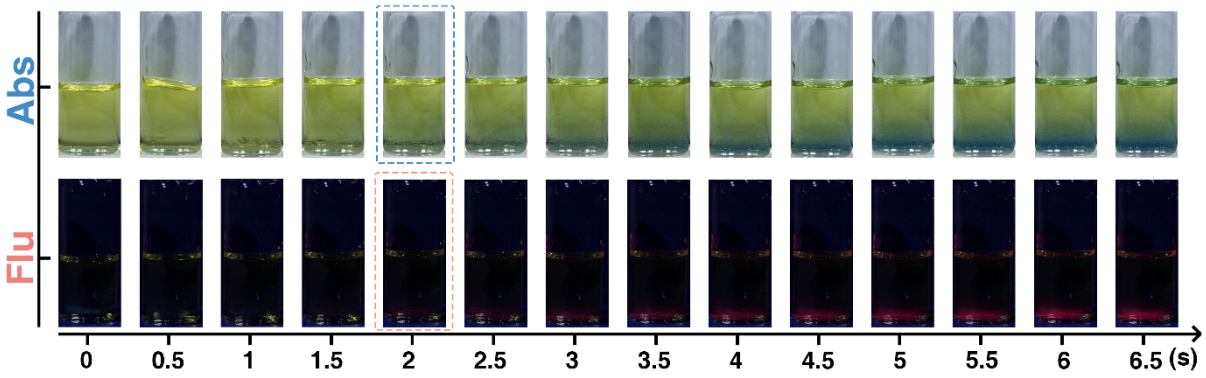

Figure S13. The time-elapse images of the [Pt(tpy-OH)Cl]·Cl solution (0.6 mM) upon addition of phosphate solution (1 mM)

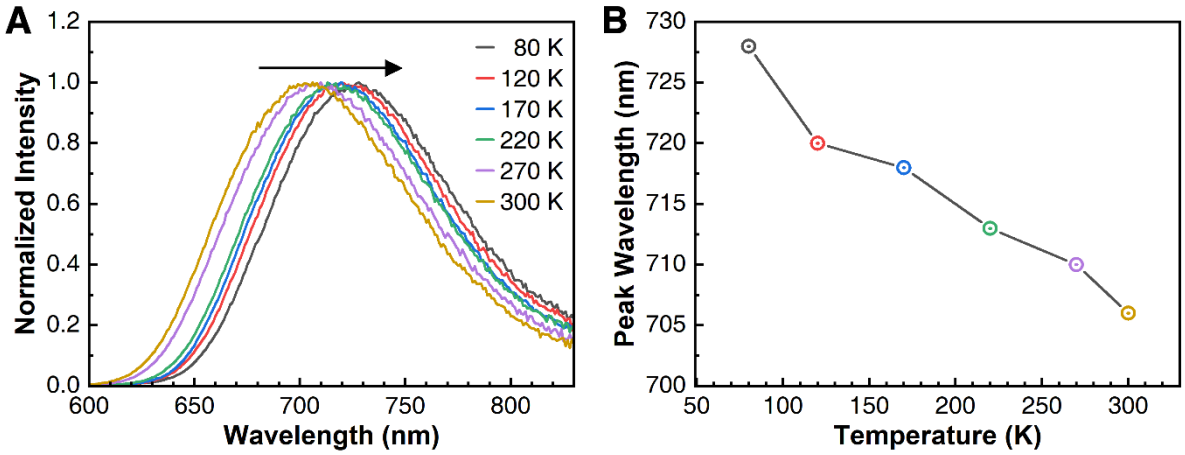

Figure S14. A) Emission spectra of the [Pt(tpy-OH)Cl]·H_2PO_4 at different temperature and B) the corresponding emission peak variation as a function of temperature

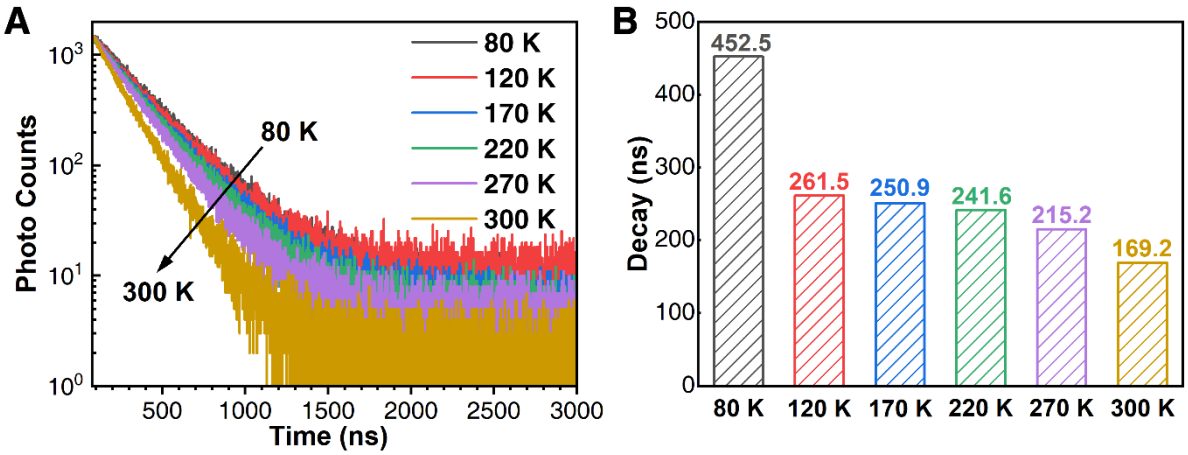

Figure S15. A) Transient PL decay profiles of the [Pt(tpy-OH)Cl]·H_2PO_4 at different temperature and B) the corresponding decay time at different temperature

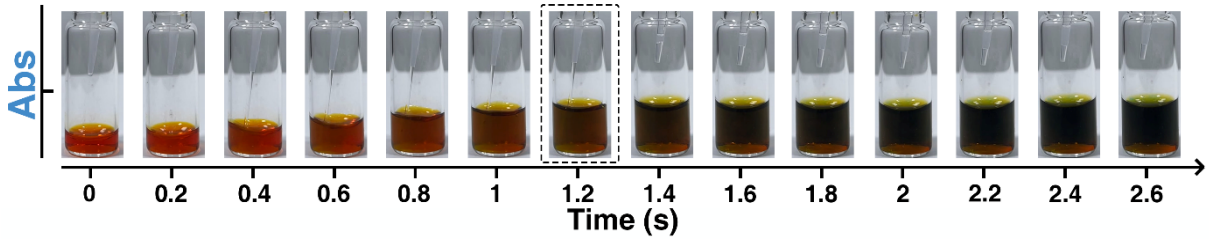

Figure S16. The time-elapse images of the the commercial reagent upon addition of phosphate solution

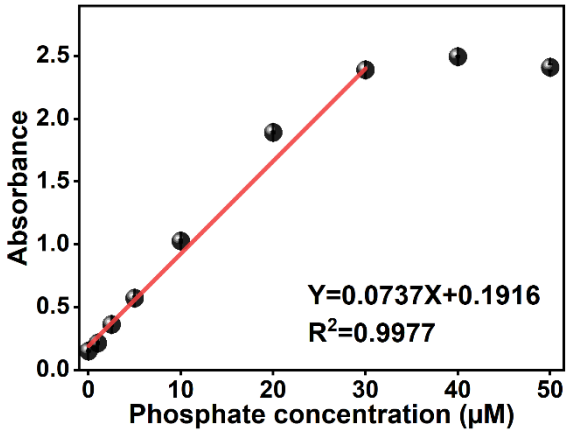

Figure S17. The absorbance of the the commercial reagent at 630 nm as a function of phosphate concentrations upon addition of phosphate solution

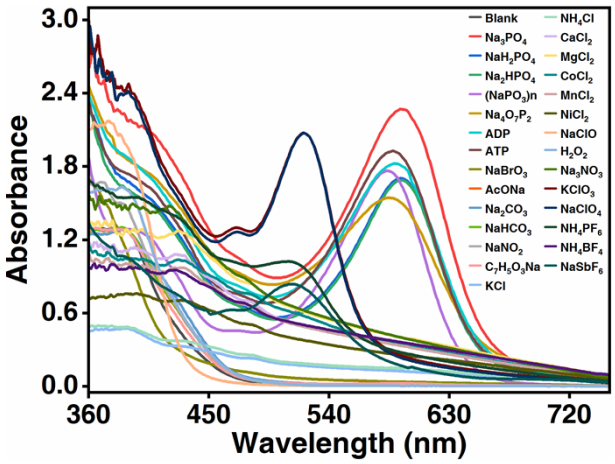

Figure S18. Absorption spectra of the selectivity test of [Pt(tpy-OH)Cl]·Cl probe solution (0.6 mM) for phosphate

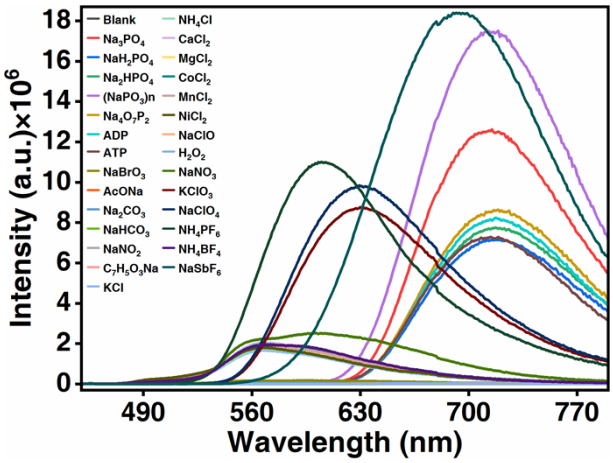

Figure S19. Fluorescent spectra of the selectivity test of [Pt(tpy-OH)Cl]·Cl probe solution (0.6 mM) for phosphate

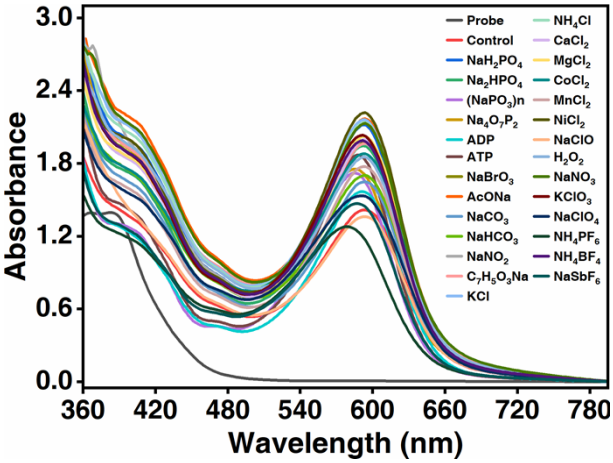

Figure S20. Absorption spectra of the anti-interference test of [Pt(tpy-OH)Cl]·Cl probe solution (0.6 mM) for phosphate

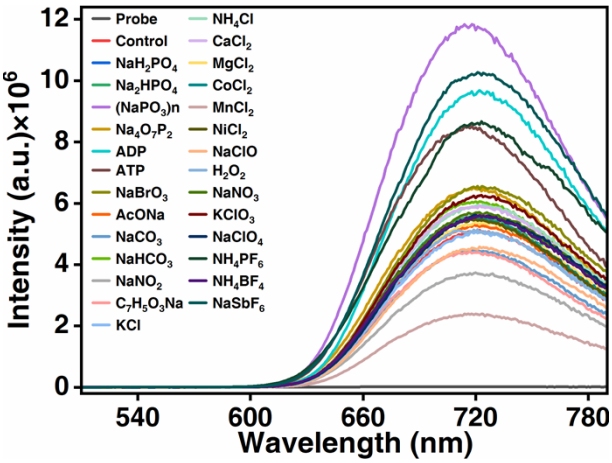

Figure S21. Fluorescent spectra of the anti-interference test of [Pt(tpy-OH)Cl]·Cl probe solution (0.6 mM) for phosphate

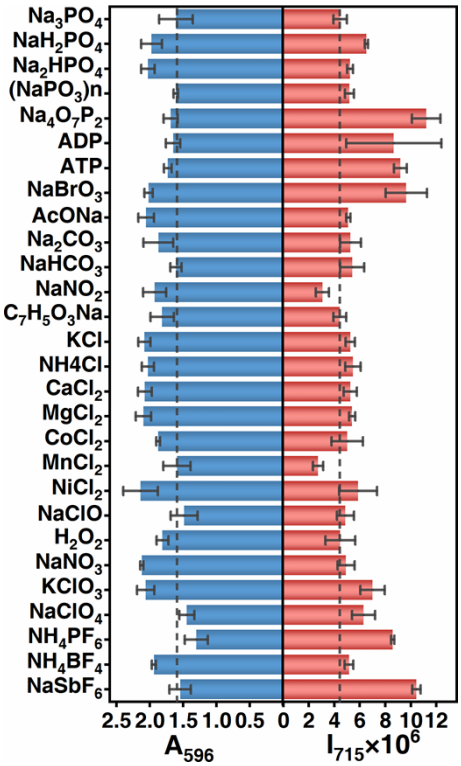

Figure S22. Histograms of absorption intensity at 596 nm and luminescence intensity at 715 nm after adding same amount of different substances along with Na_3PO_4

Table S1. Crystal data and structure refinement for [Pt(tpy-OH)Cl]·Cl

compound	**[Pt(tpy-OH)Cl]·Cl·2C_2H_6OS**
Empirical formula	$C_{19}H_{23}Cl_2N_3O_3PtS_2$
Formula weight	671.51
Temperature/K	204.00
Crystal system	monoclinic
Space group	$P2_1/n$
a/Å	6.8321(4)
b/Å	18.0865(9)
c/Å	18.6808(10)
α/°	90
β/°	95.559(2)
γ/°	90
Volume/Å^3	2297.5(2)
Z	4
ρ_{calc}g/cm^3	1.941
μ/mm^{-1}	10.555
F(000)	1304.0
Crystal size/mm^3	0.13 × 0.12 × 0.1
Radiation	GaKα (λ = 1.34139)
2Θ range for data collection/°	9.306 to 120.54
Index ranges	-8 ≤ h ≤ 8, 0 ≤ k ≤ 22, 0 ≤ l ≤ 24
Reflections collected	4769
Independent reflections	4769 [R_{int}= 0.0587, R_{sigma}= 0.0414]
Data/restraints/parameters	4769/0/277
Goodness-of-fit on F^2	1.060
Final R indexes [I>=2σ (I)]	R_1 = 0.0472, wR_2 = 0.1518
Final R indexes [all data]	R_1 = 0.0524, wR_2 = 0.1678
Largest diff. peak/hole / e Å^{-3}	2.05/-2.90

The obtained single crystal has been deposited at the Cambridge Crystallographic Data Centre and allocated the deposition number: 2331276.

Table S2.Crystal data and structure refinement for product.

compound	**2[Pt(tpy-O)Cl]·3CH_3OH**
Empirical formula	$C_{33}H_{32}Cl_2N_6O_5Pt_2$
Formula weight	1053.72
Temperature/K	193.00
Crystal system	orthorhombic
Space group	Pnna
a/Å	18.9995(14)
b/Å	13.3731(10)
c/Å	13.0869(10)
α/°	90
β/°	90
γ/°	90
Volume/$Å^3$	3325.1(4)
Z	4
$\rho_{calc}g/cm^3$	2.105
μ/mm^{-1}	11.941
F(000)	2008.0
Crystal size/mm^3	0.13 × 0.11 × 0.1
Radiation	GaKα (λ = 1.34139)
2Θ range for data collection/°	8.224 to 109.768
Index ranges	-23 ≤ h ≤ 17, -14 ≤ k ≤ 16, -15 ≤ l ≤ 15
Reflections collected	21915
Independent reflections	3168 [R_{int} = 0.0555, R_{sigma} = 0.0355]
Data/restraints/parameters	3168/10/230
Goodness-of-fit on F^2	1.044
Final R indexes [I>=2σ (I)]	R_1 = 0.0270, wR_2 = 0.0610
Final R indexes [all data]	R_1 = 0.0439, wR_2 = 0.0691
Largest diff. peak/hole / e $Å^{-3}$	0.56/-1.11

The obtained single crystal has been deposited at the Cambridge Crystallographic Data Centre and allocated the deposition number: 2331281.

Table S3. Comparison of the probe with recently reported detetion methods for phosphates

Detection manner		Materials	Response time	LOD	Ref.
Electrochemical approach		graphene		2×10^{-6}M	[15]
Colorimetry		nanozyme		4.98×10^{-8}M	[16]
Colorimetry		Ce-Zr-MOFs	5 min	1.1×10^{-6}M	[17]
Colorimetry		AgNPls		0.33mgL^{-1}	[18]
Colorimetry		Triarylmethane dye		0.07mgL^{-1}	[19]
Fluorescence turn-on		MOF	10 min	0.16×10^{-6}M	[20]
Fluorescence turn-on		polymer		4.65×10^{-6}M	[21]
Fluorescence quenching		COF		0.61×10^{-6}M	[22]
Fluorescence quenching		AgNCs		0.5×10^{-6}M	[23]
Ratiometric fluorescence		AuNCs		0.14×10^{-6}M	[24]
Ratiometric fluorescence		MOF		6.5×10^{-6}M	[25]
Dual-mode	Colorimetry	MOF		23×10^{-9}M	[26]
	Fluorometry			220×10^{-9}M	
Dual-mode	Colorimetry	Carbon dots		13.5×10^{-6}M	[27]
	Fluorometry			2.74×10^{-6}M	
Commercial reagent	colorimetry	-	1.2 s	1.6×10^{-8}M	
Dual-mode	Colorimetry	Platinum(II) complex	2s	5.73×10^{-6}M	This study
	Fluorometry			2.25×10^{-9} M	

References

[1] Basolo, F.; Gray, H. B.; Pearson, R. G., Mechanism of Substitution Reactions of Complex Ions. XVII.1 Rates of Reaction of Some Platinum(II) and Palladium(II) Complexes with Pyridine. *Journal of the American Chemical Society* **1960,** *82*, 4200-4203.

[2] Bailey, J. A.; Hill, M. G.; Marsh, R. E.; Miskowski, V. M.; Schaefer, W. P.; Gray, H. B., Electronic Spectroscopy of Chloro(terpyridine)platinum(II). *Inorganic Chemistry* **1995,** *34*, 4591-4599.

[3] Dolomanov, O. V.; Bourhis, L. J.; Gildea, R. J.; Howard, J. A. K.; Puschmann, H., OLEX2: a complete structure solution, refinement and analysis program. **2009,** *42* (2), 339-341.

[4] Sheldrick, G., SHELXT - Integrated space-group and crystal-structure determination. *Acta Crystallographica Section A* **2015,** *71*, 3-8.

[5] Sheldrick, G. M., Crystal structure refinement with SHELXL. (2053-2296 (Electronic)).

[6] Dolomanov, O. V.; Bourhis, L. J.; Gildea, R. J.; Howard, J. A. K.; Puschmann, H., OLEX2: a complete structure solution, refinement and analysis program. *Journal of Applied Crystallography* **2009,** *42*, 339-341.

[7] Bourhis, L. J.; Dolomanov, O. V.; Gildea, R. J.; Howard, J. A. K.; Puschmann, H., The anatomy of a comprehensive constrained, restrained refinement program for the modern computing environment - Olex2 dissected. *Acta Crystallographica Section A* **2015,** *71*, 59-75.

[8] Stephens, P. J.; Devlin, F. J.; Chabalowski, C. F.; Frisch, M. J., Ab Initio Calculation of Vibrational Absorption and Circular Dichroism Spectra Using Density Functional Force Fields. *The Journal of Physical Chemistry* **1994,** *98*, 11623-11627.

[9] Weigend, F.; Ahlrichs, R., Balanced basis sets of split valence, triple zeta valence and quadruple zeta valence quality for H to Rn: Design and assessment of accuracy. *Physical Chemistry Chemical Physics* **2005,** *7*, 3297-3305.

[10] Zhang, J.; Lu, T., Efficient evaluation of electrostatic potential with computerized optimized code. *Physical Chemistry Chemical Physics* **2021,** *23*, 20323-20328.

[11] Marenich, A. V.; Cramer, C. J.; Truhlar, D. G., Universal Solvation Model Based on Solute Electron Density and on a Continuum Model of the Solvent Defined by the Bulk Dielectric Constant and Atomic Surface Tensions. *The Journal of Physical Chemistry B* **2009,** *113*, 6378-6396.

[12] Lu, T.; Chen, F., Multiwfn: A multifunctional wavefunction analyzer. *Journal of Computational Chemistry* **2012,** *33*, 580-592.

[13] Humphrey, W.; Dalke, A.; Schulten, K., VMD: Visual molecular dynamics. *Journal of Molecular Graphics* **1996,** *14*, 33-38.

[14] M. J. Frisch, G. W. Trucks, H. B. Schlegel, G. E. Scuseria, M. A. Robb, J. R. Cheeseman, G. Scalmani, V. Barone, G. A. Petersson, H. Nakatsuji, X. Li, M. Caricato, A. V. Marenich, J. Bloino, B. G. Janesko, R. Gomperts, B. Mennucci, H. P. Hratchian, J. V. Ortiz, A. F. Izmaylov, J. L. Sonnenberg, Williams, F. Ding, F. Lipparini, F. Egidi, J. Goings, B. Peng, A. Petrone, T. Henderson, D. Ranasinghe, V. G. Zakrzewski, J. Gao, N. Rega, G. Zheng, W. Liang, M. Hada, M. Ehara, K. Toyota, R. Fukuda, J. Hasegawa, M. Ishida, T. Nakajima, Y. Honda, O. Kitao, H. Nakai, T. Vreven, K. Throssell, J. A. Montgomery Jr., J. E. Peralta, F. Ogliaro, M. J. Bearpark, J. J. Heyd, E. N. Brothers, K. N. Kudin, V. N. Staroverov, T. A. Keith, R. Kobayashi, J. Normand, K. Raghavachari, A. P. Rendell, J. C. Burant, S. S. Iyengar, J. Tomasi, M. Cossi, J. M. Millam, M. Klene, C. Adamo, R. Cammi, J. W. Ochterski, R. L. Martin, K. Morokuma, O. Farkas, J. B. Foresman, D. Fox, Gaussian 16, Revision C.01, Gaussian, Inc., Wallingford, CT 2016.

[15] Li, S.-N.; You, Y.; Hu, W.-G.; Gao, G.-J.; Jiang, X.-Y.; Yu, J.-G., A sensitive single-layered graphene oxide-based sensor for electrochemical sensing of phosphate anion. *Process Safety and Environmental Protection* **2023,** *178*, 786-794.

[16] Li, X.; Liu, B.; Ye, K.; Ni, L.; Xu, X.; Qiu, F.; Pan, J.; Niu, X., Highly sensitive and specific colorimetric detection of phosphate by using Zr (IV) to synergistically suppress the peroxidase-mimicking activity of hydrophilic Fe_3O_4 nanocubes. *Sensors and Actuators B-Chemical* **2019,** *297*, 126822.

[17] Li, X.; Niu, X.; Liu, P.; Xu, X.; Du, D.; Lin, Y., High-performance dual-channel ratiometric colorimetric sensing of phosphate ion based on target-induced differential oxidase-like activity changes of Ce-Zr bimetal-organic frameworks. *Sensors and Actuators B-Chemical* **2020,** *321*, 128546.

[18] Pinyorospathum, C.; Rattanarat, P.; Chaiyo, S.; Siangproh, W.; Chailapakul, O., Colorimetric sensor for determination of phosphate ions using anti-aggregation of 2-mercaptoethanesulfonate-modified silver nanoplates and europium ions. *Sensors and Actuators B-Chemical* **2019,** *290*, 226-232.

[19] Choudhary, V.; Philip, L., Stable paper-based colorimetric sensor for selective detection of phosphate ion in aqueous phase. *Microchemical Journal* **2021,** *171*, 106809.

[20] Zhang, G.; Ma, Y.; Chai, H.; Yu, K.; Li, Y.; Wang, S.; Ma, J.; Qu, L.; Tan, W.; Zhang, X., Porphyrinic metal-organic framework@alumina nanocomposite fluorescent probe: Two-stage stimuli-responsive behavior and phosphate sensing. *Sensors and Actuators B-Chemical* **2022,** *370*, 132395.

[21] Zhao, C.-X.; Zhang, X.-P.; Shu, Y.; Wang, J.-H., Europium-Pyridinedicarboxylate-Adenine Light-Up Fluorescence Nanoprobes for Selective Detection of Phosphate in Biological Fluids. *ACS Applied Materials & Interfaces* **2020,** *12*, 22593-22600.

[22] Afshari, M.; Dinari, M.; Farrokhpour, H.; Zamora, F., Imine-Linked Covalent Organic Framework with a Naphthalene Moiety as a Sensitive Phosphate Ion Sensing. *ACS Applied Materials & Interfaces* **2022,** *14*, 22398-22406.

[23] Farahani, S. M.; Dadmehr, M.; Karimi, M. A.; Korouzhdehi, B.; Karimi, M. A.; Rajabian, M., Fluorometric detection of phytase enzyme activity and phosphate ion based on gelatin supported silver nanoclusters. *Food Chemistry* **2022,** *396*, 133711.

[24] Zhang, Z.; Feng, J.; Huang, P.; Li, S.; Wu, F.-Y., Ratiometric fluorescent detection of phosphate in human serum with functionalized gold nanoclusters based on chelation-enhanced fluorescence. *Sensors and Actuators B-Chemical* **2019,** *298*, 126891.

[25] Yi, K.; Zhang, X.; Zhang, L., Smartphone-based ratiometric fluorescent definable system for phosphate by merged metal-organic frameworks. *Science of the Total Environment* **2021,** *772*, 144952.

[26] Cheng, C.; Zhang, R.; Wang, J.; Zhang, Y.; Xiong, S.; Huang, Y.; Yang, M., Porphyrinic Metal-Organic Framework Nanorod-Based Dual-Modal Nanoprobe for Sensing and Bioimaging of Phosphate. *ACS Applied Materials & Interfaces* **2020,** *12*, 26391-26398.

[27] Li, X.; Ding, S.; Lyu, Z.; Tieu, P.; Wang, M.; Feng, Z.; Pan, X.; Zhou, Y.; Niu, X.; Du, D.; Zhu, W.; Lin, Y., Single-Atomic Iron Doped Carbon Dots with Both Photoluminescence and Oxidase-Like Activity. *Small* **2022,** *18*, e2203001.